Lossy Point Cloud Attribute Compression with Subnode-Based Prediction

YIN Qian[1], ZHANG Xinfeng[2], HUANG Hongyue[1], WANG Shanshe[1], MA Siwei[1]
(1. School of Computer Science, Peking University, Beijing 100871, China;
2. School of Computer Science and Technology, University of the Chinese Academy of Sciences, Beijing 100049, China)

DOI: 10.12142/ZTECOM.202304004
https: //kns.cnki.net/kcms/detail/34.1294.TN.20231122.1025.002.html, published online November 23, 2023
Manuscript received: 2023-10-07

Abstract: Recent years have witnessed that 3D point cloud compression (PCC) has become a research hotspot both in academia and industry. Especially in industry, the Moving Picture Expert Group (MPEG) has actively initiated the development of PCC standards. One of the adopted frameworks called geometry-based PCC (G-PCC) follows the architecture of coding geometry first and then coding attributes, where the region adaptive hierarchical transform (RAHT) method is introduced for the lossy attribute compression. The upsampled transform domain prediction in RAHT does not sufficiently explore the attribute correlations between neighbor nodes and thus fails to further reduce the attribute redundancy between neighbor nodes. In this paper, we propose a subnode-based prediction method, where the spatial position relationship between neighbor nodes is fully considered and prediction precision is further promoted. We utilize some already-encoded neighbor nodes to facilitate the upsampled transform domain prediction in RAHT by means of a weighted average strategy. Experimental results have illustrated that our proposed attribute compression method shows better rate-distortion (R-D) performance than the latest MPEG G-PCC (both on reference software TMC13-v22.0 and GeS-TM-v2.0).

Keywords: point cloud compression; MPEG G-PCC; RAHT; subnode-based prediction

Citation (Format 1): YIN Q, ZHANG X F, HUANG H Y, et al. Lossy point cloud attribute compression with subnode-based prediction [J]. ZTE Communications, 2023, 21(4): 29 - 37. DOI: 10.12142/ZTECOM.202304004
Citation (Format 2): Q. Yin, X. F. Zhang, H. Y. Huang, et al., "Lossy point cloud attribute compression with subnode-based prediction," *ZTE Communications*, vol. 21, no. 4, pp. 29 - 37, Dec. 2023. doi: 10.12142/ZTECOM.202304004.

1 Introduction

Rapid progress in 3D graphic technologies and capture devices has enabled high-precision digital representations of 3D objects or scenes. Point clouds, as one of the mainstream 3D data formats, can effectively indicate points in real-world scenes through 3D geometric coordinates and corresponding attributes (e.g., color, normal and reflectance). Considering its flexible representation properties, point clouds have been widely applied to various fields, such as autonomous driving, free-viewpoint broadcasting, and heritage reconstruction[1]. However, in addition to a huge amount of data, point clouds are non-uniformly sampled in space, which undoubtedly makes it unfeasible to put point clouds into applications with limited bandwidth and storage space[2]. Therefore, it is necessary to investigate efficient point cloud compression (PCC) schemes.

With an increasing demand for point cloud applications, the Moving Picture Expert Group (MPEG) standardization committee started to conduct PCC-dedicated standards and issued a Call for Proposals (CfP) in 2017[3]. After intensive developments involving academic and industrial meetings, two independent point cloud compression frameworks have been adopted to cover a wider range of immersive applications and data types. One called video-based PCC (V-PCC)[4] adopts projection-based strategies combined with video codecs, which aims for handling dense point clouds. Another called geometry-based PCC (G-PCC)[5] is more specifically designed for relatively sparse point clouds by using the octree-based architecture. The octree representation first proposed for PCC in Ref. [6] can build a progressive 3D structure for point clouds. Specifically, by recursively dividing point clouds from the root node to leaf nodes, the connectivity information between points can be exploited among the unorganized point clouds. Moreover, the topological neighbor information makes it easier to implement techniques similar to prediction or transformation in video coding. In the current G-PCC scheme, geometry and attributes are coded sequentially and multiple coding tools can be selected to suit different application scenarios.

This work was supported in part by China Postdoctoral Science Foundation under Grant No. 2022M720234 and in part by the National Natural Science Foundation under Grant Nos. 62071449 and U21B2012.

For the geometry information, in addition to octree coding[7], the triangle soup (Trisoup) coding[8] is used to approximate the surface of point clouds as a complement to the octree decomposition while predictive tree coding[9] is applied to low-delay use cases. In terms of attributes, there are mainly two branches concerning different advantages. The level of details (LODs)-based prediction scheme[10] aims to near-lossless or lossless compression and also deliver spatial scalability to G-PCC. By contrast, the region adaptive hierarchical transform (RAHT) scheme[11] is more suitable for lossy compression with much lower complexity. Note that the attribute coding framework RAHT is our main focus in this paper.

As the mainstream attribute compression scheme, the RAHT was first proposed in Ref. [12] to provide a hierarchical transform structure. In general, the RAHT is an adaptive variant of the Haar wavelet transform (HWT), which can evolve into a 3D version of the Haar transform when all nodes are occupied. To furthermore improve the coding efficiency of the RAHT, an upsampled transform domain prediction[13] was proposed and has been adopted in the current G-PCC. Specifically, decoded attributes of the nodes at lower levels (i.e., lower resolution) are used to predict attributes of the nodes at higher levels. Then, the prediction residuals can be further quantized and entropically encoded. During the transform domain prediction stage, in addition to the nodes at lower levels, the nodes at current encoding levels can also be applied to prediction by means of weighted average[14]. However, the information of surrounding neighbor nodes has not been fully utilized in certain search ranges, which means that further exploring the correlations between neighbor nodes can lead to better attribute compression performance.

In this paper, we propose a subnode-based prediction scheme for point cloud attribute compression, which aims at optimizing the upsampled transform domain prediction in RAHT. Specifically, we first analyze the spatial distribution among neighbor nodes and further explore their reference relationship. Based on this analysis, the prediction accuracy is further improved by exploiting some already-encoded nodes that are not used in the current prediction. Then, a weighted average strategy is introduced for the final attribute prediction of the node to be encoded. Extensive simulations are conducted and compared with the G-PCC as the anchor. Experimental results have confirmed that our proposed method outperforms both Test Model Category 13 (TMC13) and Geometry-Based Solid Content Test Model (GeS-TM) platforms in terms of all point cloud datasets provided by MPEG.

The remainder of this paper is organized as follows. Section 2 succinctly reviews the related works on attribute coding in PCC and describes the current RAHT scheme of G-PCC in particular. Our proposed subnode-based prediction approach is then presented in Section 3. Section 4 provides experimental results and analysis and Section 5 concludes this paper.

2 Related Work

In this section, we first review the attribute coding schemes for PCC. They can be mainly divided into three categories, which are projection-based methods, prediction-based methods and transform-based methods. All of them have been introduced to the MPEG PCC standards. To be more specific, the V-PCC utilizes projection-based methods while the other two strategies have been adopted by the G-PCC. Since our work mainly focuses on the geometry-based PCC, the research related to video-based PCC is outside the scope of this paper. Moreover, the current RAHT scheme and upsampled transform domain prediction of G-PCC are also specifically described as our background.

2.1 Point Cloud Attribute Coding Technologies

Among the existing attribute coding approaches, the prediction-based technology is one of the popular schemes to exploit spatial attribute correlations between points. For example, the attribute prediction framework in G-PCC[10] introduces a linear interpolation process by using the k-nearest neighbors (KNN) search algorithm. This prediction method is based on a LODs structure, which splits the whole point cloud into several subsets (i.e., refinement levels) according to the distance criterion. Based on the LODs, the point clouds are then reordered and encoded, where attributes of points are always predicted by their KNN in the previous LODs. Furthermore, an additional flag is provided in Ref. [15] to allow predictions by using points at the same level. On top of the prediction framework, a lifting scheme[16] is proposed to promote attribute lossy coding. To be more specific, compared with the original prediction method, an update operator combined with an adaptive quantization strategy is added to improve the prediction accuracy. Attributes of points in lower LODs are always assigned much higher influence weights because they are used as reference points with higher frequency and probability for predicting points in higher LODs.

Based on the above two prediction schemes, substantial works are investigated to further improve the attribute compression efficiency. WEI et al. propose an enhanced intra-prediction scheme[17] by considering the overall geometric distribution of the neighbors set. They introduce the centroid-based criterion to measure the distribution uniformity of points in a predictive reference set. Since this scheme predictively encodes the point clouds point by point, the prediction errors will accumulate and propagate, especially for points in higher LODs. Hence, a bilateral filter is proposed in Ref. [18] to update the reconstruction values of decoded points, which reduces error propagation when encoding subsequent points. In addition, YIN et al. attempt to optimize the predictive neighbor set by using the normal of point clouds[19], aiming at improving prediction precision for Light Detection and Ranging (LiDAR) point clouds.

Besides prediction-based methods, other approaches con-

tribute to reducing the attribute spatial redundancy in a transform domain. For instance, to utilize the 2D discrete cosine transform (DCT), ZHANG et al. project the point clouds onto two-dimensional grids for color compression[20]. This 3D-to-2D-based method inevitably fails to fully consider three-dimensional spatial correlations. Hence, 3D-DCT-based methods are developed continuously, such as Refs. [21] and [22].

Apart from DCT, more complex transforms are introduced to attribute coding for PCC. The graph Fourier transform (GFT) is first applied to PCC in Ref. [23], which is an extension of the Karhunen-Loève transform (KLT). The graphs are constructed based on octree-decomposed point clouds, where the graph Laplacian matrix can be deduced by connecting the points within small neighborhoods. Then attributes are transformed, quantized, and entropically encoded. Since the coding efficiency of the graph-based methods outperforms the DCT-based method, extensive follow-up works have been carried out on the attribute graph transform coding. Specifically, an optimized graph transform method[24] is proposed to improve the Laplacian sparsity combined with k-dimensional tree partition and an RDO-based quantization process. Then, XU et al.[25] introduce the normal of point clouds, in addition to geometric distance, to measure the connectivity between neighbor points. Moreover, they propose a predictive generalized graph transform scheme[26] to eliminate the temporary redundancy. Although the graph-based transform approaches exhibit superior coding performance, complicated matrix decomposition leads to real-time difficulties in PCC.

Taking the complexity into consideration, RAHT is proposed in Ref. [12] and finally adopted in G-PCC as the fundamental framework. Our work is closely related to the RAHT and corresponding techniques, which will be concisely described in Section 2.2.

2.2 RAHT in MPEG G-PCC

RAHT is a Haar-inspired method with a hierarchical structure, which can be regarded as an extension of 1D HWT. The core of HWT is to represent functions and signals by using a series of wavelets or basis functions. Specifically, suppose a signal S has N elements. The HWT decomposes the original signal S into low-pass and high-pass components, which can be calculated as follows:

$$\begin{bmatrix} \mathrm{DC} \\ \mathrm{AC} \end{bmatrix} = \frac{1}{\sqrt{2}} \begin{bmatrix} 1 & 1 \\ -1 & 1 \end{bmatrix} \begin{bmatrix} S_{2n} \\ S_{2n+1} \end{bmatrix}, \tag{1}$$

where S_{2n} and S_{2n+1} denote two adjacent elements of signal s. The direct current (DC) and alternating current (AC) coefficients represent the low-frequency and high-frequency parts of the signal respectively. Generally speaking, the energy of the signal after the HWT is mainly concentrated on a few coefficients, especially the DC coefficients, and then appropriate quantization and entropy coding can achieve the purpose of compression.

In order to apply HWT for 3D point cloud attribute compression, 1D HWT is applied sequentially along the x, y, and z directions. Specifically, the RAHT is conducted on a hierarchical octree based on the geometry information of point clouds, which starts from the leaf nodes (i.e., highest resolution level) and proceeds backward until the octree's root node (i.e., lowest resolution level). In each level, the RAHT is applied to each unit node containing 2×2×2 subnodes. As shown in Fig. 1, the unit node is transformed along three directions to generate both DC and AC coefficients, where the DC coefficients along each direction will continue to be transformed while the AC coefficients will be output to be quantized and encoded. Note that the number of coefficients is the same as the number of occupied subnodes in a unit node, including one DC coefficient and several AC coefficients. Then, the DC coefficient obtained from the node at Level l will be used as the attribute of the node at Level l-1 for further transformation. After processing all unit nodes (N occupied nodes) at Level l, N generated DC coefficients (denoted as LLL) continue to be transformed until the root node.

It should be noted that, in the current G-PCC, the dyadic RAHT decomposition[27] is adopted to adapt to more complicated textures. The whole process of the dyadic RAHT is exactly the same as the normal RAHT mentioned above, except that the AC coefficients obtained in each direction will be further transformed like the DC coefficients. Another point to be emphasized is that, unlike HWT in Eq. (1), the wavelet transform kernel for RAHT is modified according to

$$\mathrm{RAHT}(w_1, w_2) = \frac{1}{\sqrt{w_1 + w_2}} \begin{bmatrix} \sqrt{w_1} & \sqrt{w_2} \\ -\sqrt{w_2} & \sqrt{w_1} \end{bmatrix}, \tag{2}$$

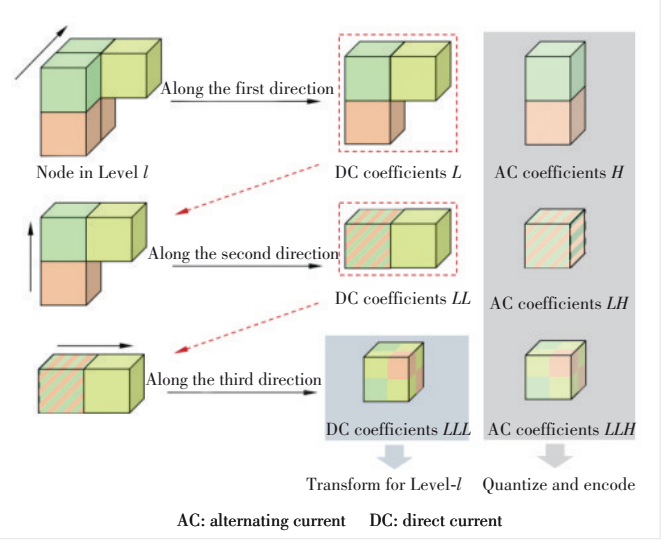

▲ **Figure 1. Transform procedure of a unit node along three directions. The DC coefficient is denoted as *L* and *H* represents the AC coefficient. *LL* and *LH* represent the DC coefficient and AC coefficient of DC coefficient respectively, and so on**

where w_1 and w_2 represent the number of points in two adjacent nodes, which makes the transform more adaptive to the sparsity of point clouds.

To further explore the local spatial correlation, the inter-depth upsampling (IDUS) method[13] is proposed to predict attributes of nodes in the transform domain. As shown in Fig. 2, the upsampling process is realized by means of a weighted average based on geometric distance in the mean attribute space. During the prediction procedure, for each node at Level l, there are mainly two types of nodes used for prediction, which are parent-level neighbors at Level l-1 and subnode-level neighbors at Level l[14]. However, there are still some already-encoded neighbors that are not utilized in the current prediction and the prediction reference relationship can be further refined to improve the attribute compression efficiency.

3 Proposed Approach

Based on the framework described in Section 2.2, we propose a subnode-based transform domain prediction for RAHT that considers more accurate spatial correlations among nodes. In addition to the parent-level neighbors and subnode-level neighbors in G-PCC, some other effective neighbors are also utilized for upsampled transform domain prediction. As illustrated in Fig. 3, the parent-level neighbors at level l-1 include three types of nodes, which are the parent node (*Npm*), co-plane parent neighbor node (sharing a side with the subnode to be predicted, *Ncppnn*), and co-line parent neighbor node (sharing an edge with the subnode to be predicted, *Nclpnn*). For the subnode-level neighbors at Level l, there are the co-plane subnode in the co-plane parent neighbor node (*Ncpsn*), co-line subnode in the co-line parent neighbor node (*Nclsncl*) and proposed co-line subnode in the co-plane parent neighbor node (*Nclsncp*). With these predictive reference nodes, we design an optimized transform domain prediction for RAHT. Compared with the original prediction scheme in G-PCC, we first introduce already-encoded neighbor nodes *Nclsncp* as reference candidates and the neighbor search for nodes *Nclsncp* is described in Section 3.1. Since a new type of predictive reference neighbors is added, we further propose a geometric distribution-based prediction to refine the original node prediction reference relationship, which is then detailed in Section 3.2.

Type	Description	Symbols in Diagram
Parent-level nodes in Level l-1	Parent node Co-plane parent neighbor node Co-line parent neighbor node	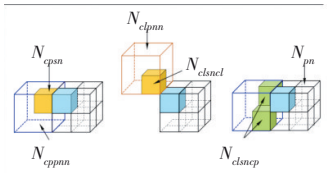
Subnode-level nodes in Level l	Co-plane subnode Co-line subnode in N_{clpnn} **Co-line subnode in N_{cppnn}**	

▲ **Figure 3. Notations of different types of nodes for transform domain prediction, which include parent-level neighbor nodes at level l-1 and subnode-level neighbor nodes at level l**

3.1 Neighbor Search for Reference Candidates

Since the proposed co-line subnodes (*Nclsncp*) exist in the co-plane parent neighbor nodes (*Ncppnn*), the neighbor search is mainly decomposed into two stages: 1) determining the co-plane parent neighbor nodes and 2) deciding co-line subnodes reference candidates. Specifically, for each subnode to be predicted, the corresponding parent node has at most six co-plane parent neighbor nodes. Among them, already-encoded subnodes *Nclsncp* can only exist in three parent neighbor nodes (Fig. 4), which are located on the left, front and bottom of *Npn* respectively.

Further considering the position of each subnode to be predicted in its *Npn* as well as the distribution of corresponding *Ncppnn*, the detailed existence of *Nclsncp* of each subnode to be predicted is shown in Fig. 4. Note that the position indexes (from 0 to 8) are organized according to the Morton order. Specifically, we denote *Ntbp* i as the i-th subnode to be predicted in the same *Npn*. Then, it can be seen that only *Ntbp* 0 contains six

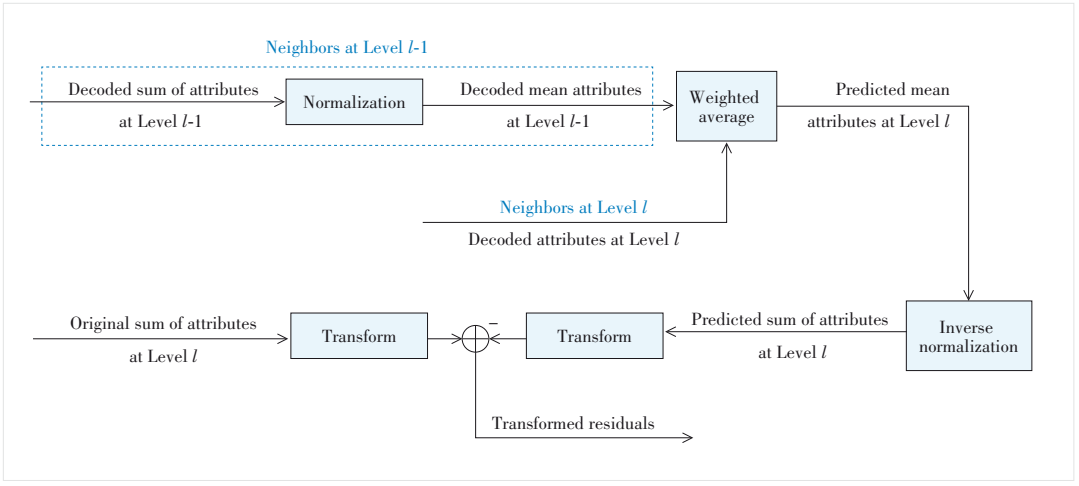

▲ **Figure 2. Upsampled transform domain prediction for region adaptive hierarchical transform (RAHT) in geometry-based point cloud compression (G-PCC), where upsampling prediction is performed in the mean attribute space and transformation is performed in the sum attribute space**

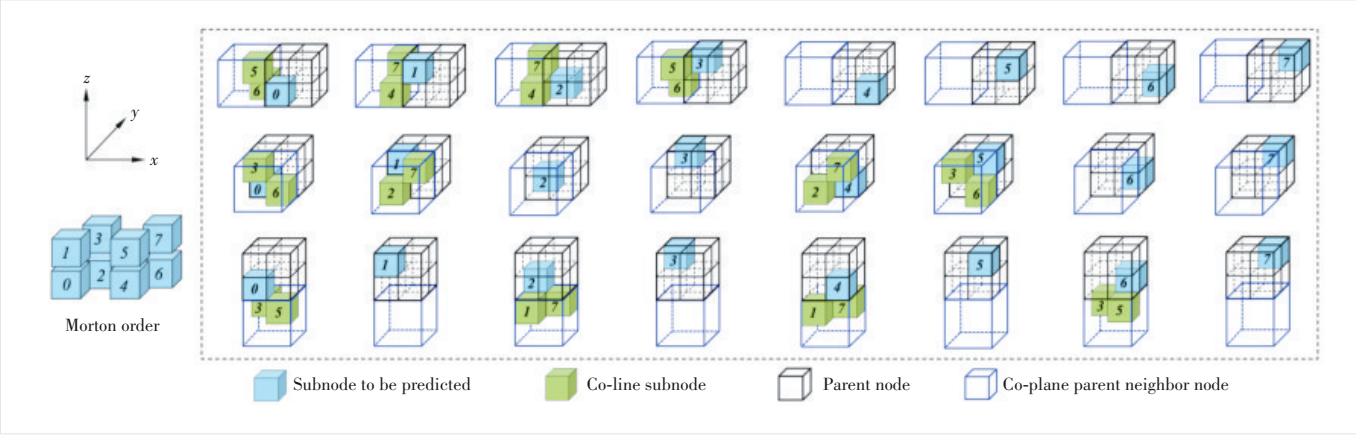

▲**Figure 4. Schematic diagram of co-line subnodes of each subnode to be encoded in the same parent node, where the position indexes are organized according to the Morton order**

Nclsncp reference candidates. *Ntbp* 1, *Ntbp* 2 and *Ntbp* 4 include four *Nclsncp* reference candidates. *Ntbp* 3, *Ntbp* 5 and *Ntbp* 6 include two *Nclsncp* reference candidates. *Ntbp* 7 has no *Nclsncp* reference candidate. More detailed information is listed as follows:

• *Ntbp* 0 candidates located in No. 5 and No. 6 subnodes of the left *Ncppnn*, No. 3 and No. 5 subnodes of the bottom *Ncppnn*, and No. 3 and No. 6 subnodes of the front *Ncppnn*.

• *Ntbp* 1 candidates located in No. 4 and No. 7 subnodes of the left *Ncppnn* and No. 2 and No. 7 subnodes of the front *Ncppnn*.

• *Ntbp* 2 candidates located in No. 4 and No. 7 subnodes of the left *Ncppnn* and No. 1 and No. 7 subnodes of the bottom *Ncppnn*.

• *Ntbp* 3 candidates located in No. 5 and No. 6 subnodes of the left *Ncppnn*.

• *Ntbp* 4 candidates located in No. 2 and No. 7 subnodes of the front *Ncppnn* and No. 1 and No. 7 subnodes of the bottom *Ncppnn*.

• *Ntbp* 5 candidates located in No. 3 and No. 6 subnodes of the front *Ncppnn*.

• *Ntbp* 6 candidates located in No. 3 and No. 5 subnodes of the bottom *Ncppnn*.

Among these reference candidates described above, the existing occupied (i. e., non-empty node) *Nclsncp* can be searched by using the relative position relationship with each corresponding *Ntbp i*. In addition to the proposed *Nclsncp*, we also introduce a prediction scheme based on geometric distribution by using *Npn*, *Ncppnn* and *Nclpnn* at Level *l*-1 and *Ncpsn* and *Nclsncl* at Level *l*, which will be detailed in the next section.

3.2 Prediction Based on Geometric Distribution

For each subnode to be predicted *Ntbp i* in its parent node *Npn*, we propose to predict them according to the distribution of their neighbor subnodes in the co-plane parent node neighbor nodes. First of all, the distribution can be mainly divided into the following three categories, a total of six subcategories, mainly including:

• Distribution 1: The existing *Ncppnn* contains *Ncpsn*, including three cases: 1) only one *Ncpsn*, 2) one *Ncpsn* and one *Nclsncp*, and 3) one *Ncpsn* and two *Nclsncp*.

• Distribution 2: The existing *Ncppnn* does not contain *Ncpsn* but contains at least one *Nclsncp*, including two cases: 1) only one *Nclsncp* and 2) two *Nclsncp*.

• Distribution 3: The existing *Ncppnn* does not contain any of *Ncpsn* and *Nclsncp*.

Then, the corresponding target prediction mode can be determined by the three types of neighbor subnode distributions. For each subnode to be predicted, in addition to their *Npn* that will definitely participate in the prediction, the prediction reference of other nodes is shown in Fig. 5. Specifically, for *Ncppnn*, we will first determine whether it contains *Ncpsn*, and if so (i.e., satisfying Distribution 1), the attribute value of *Ncpsn* will be used as the prediction instead of the attribute value of its corresponding *Ncppnn* whether it contains *Nclsncp* or not. Then, if there is no *Ncpsn* in *Ncppnn*, we further determine whether it contains at least *Nclsncp*, and if so (i.e., satisfying Distribution 2), the average attribute value of *Nclsncp* will be used as the prediction instead of the attribute value of its corresponding *Ncppnn*. If it contains neither of the above two conditions (i.e., satisfying Distribution 3), the attribute value of *Ncppnn* will be directly used for prediction. Besides *Ncppnn*, for *Ncppnn*, the attribute value of *Nclsncl* will be used as the prediction instead of the attribute value of its corresponding *Nclpnn* if it has *Nclsncl*, which is the same as the current G-PCC.

4 Experiments

To validate the effectiveness of the proposed method, we implement our subnode-based prediction scheme on top of the latest MPEG G-PCC reference software TMC13-v22.0[28] and GeS-TM-v2.0[29]. Extensive simulations have been conducted in accordance with the common test conditions (CTCs) [30]

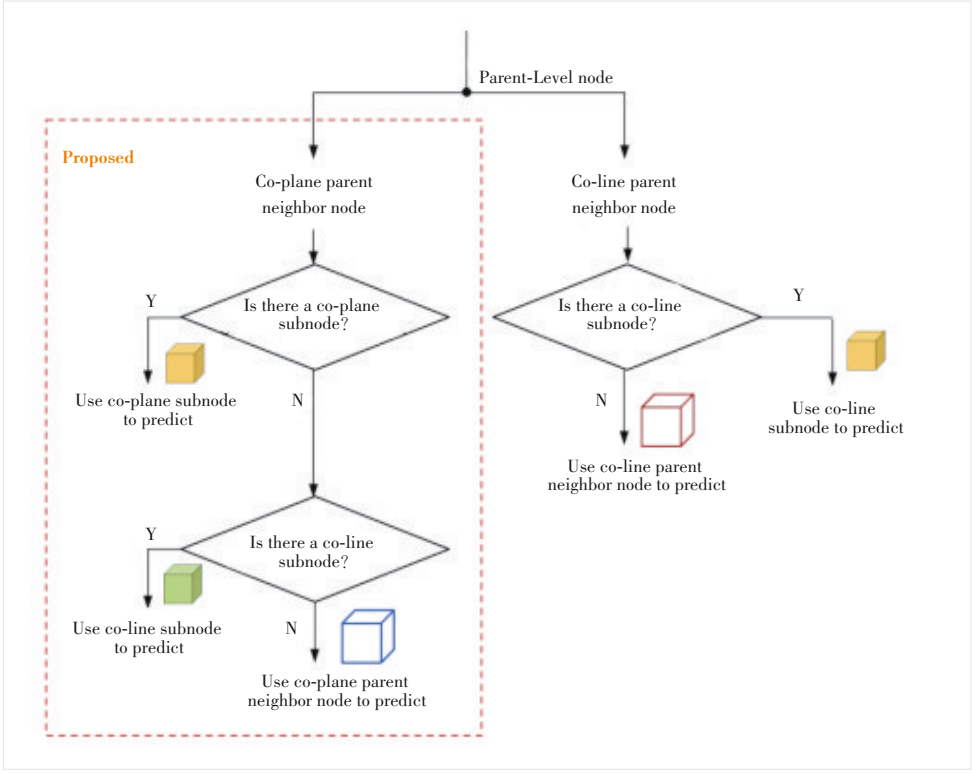

▲Figure 5. Transform domain prediction based on the three types of neighbor subnode geometric distributions

where the octree and RAHT configuration are applied for geometry and attribute respectively. In terms of the test conditions, as shown in Table 1, C1 (i.e., lossless geometry lossy attributes) and C2 conditions (i.e., near-lossless/lossy geometry lossy attributes) are both evaluated on the reference software TMC13-v22.0 and GeS-TM-v2.0.

▼Table 1. Common test conditions in G-PCC

G-PCC Platform	Conditions		Datasets		
	C1	C2	Cat1	Cat2	Cat3
TMC13	√	√	√		√
GeS-TM	√	√		√	

G-PCC: geometry-based point cloud compression

4.1 Datasets

The test datasets provided by MPEG G-PCC can be mainly classified into three categories: Category 1—Static Objects and Scenes datasets (i.e., Cat1), Category 2—Dynamic Objects datasets (i.e., Cat2), and Category 3—Dynamic Acquisition datasets (i.e., Cat3). Specifically, sequences in Cat1 are further divided based on the density and surface continuity of point clouds (i.e., Solid, Dense, Sparse, and Scant). For Cat2, test classes A, B and C indicate the complexity of point clouds, where A is the lowest and C is the highest. The division of Cat3 is more detailed, including automotive frame-based data acquired by spinning and non-spinning LiDAR sensors (i.e., Am-frame) and automotive LiDAR acquired data after fused and reprocessed (i.e., Am-fused). Note that Am-fused datasets have both color and reflectance attributes. In terms of the CTCs, the Cat1 and Cat3 datasets are tested on TMC13v22.0 while the Cat2 datasets are tested on GeS-TMv2.0. All test sequences mentioned above are available in the MPEG content repository[31].

4.2 Performance Evaluations

The attribute compression performances compared with TMC13-v22.0 are shown in Table 2, where the negative Bjontegaard delta (BD) rate illustrates the coding gains against the anchor. From Table 2, it can be seen that consistent coding

▼Table 2. Performance of the proposed method against TMC13-v22.0 under C1 and C2 configurations

Dataset Category	C1 End-to-End BD-Attribute Rate/%				C2 End-to-End BD-Attribute Rate/%			
	Luma	Chroma Cb	Chroma Cr	Reflectance	Luma	Chroma Cb	Chroma Cr	Reflectance
Solid average	−0.4	−0.3	−0.4	/	−0.2	−0.3	−0.2	/
Dense average	−0.2	−0.2	−0.2	/	−0.2	−0.5	−0.1	/
Sparse average	−0.2	−0.2	−0.1	/	−0.2	−0.1	−0.3	/
Scant average	−0.2	−0.2	−0.3	/	−0.2	−0.3	−0.2	/
Am-fused average	−0.3	−1.2	−1.1	−1.1	−0.1	−0.6	−0.7	−0.2
Am-frame spinning average	/	/	/	−0.3	/	/	/	−0.2
Am-frame non-spinning average	/	/	/	−0.6	/	/	/	−0.2
Overall average	**−0.2**	**−0.3**	**−0.3**	**−0.5**	**−0.2**	**−0.3**	**−0.2**	**−0.2**
Average encoding/decoding time/%	102/103				100/107			

BD: Bjontegaard delta

gains can be achieved both under C1 and C2 conditions for all categories. Specifically, 0.2%, 0.3% and 0.5% bitrate reduction for luma, chorma and reflectance are obtained under the C1 condition respectively. 0.2%, 0.3% and 0.2% bitrate reduction for luma, chroma Cb and Cr as well as 0.2% bitrate reduction for reflectance are obtained under C2 condition respectively. Especially for Am-fused datasets, there are over 1% coding gains under the C1 condition for chroma Cb (1.2%), chroma Cr (1.1%) and reflectance (1.1%). Besides the R-D performance, the computational complexity is evaluated by using the average encoding and decoding time. There are only 2% and 3% extra increases on the encoding and decoding time on the C1 condition, with no complexity increase for encoding on the C2 condition.

Apart from TMC13-v22.0, we also compare our proposed method with GeSTM-v2.0 for Cat2. As shown in Table 3, consistent coding gains can be also achieved both under C1 and C2 conditions for all Cat2 datasets. Specifically, 0.4%, 0.4% and 0.5% bitrate reduction for luma, chroma Cb and chroma Cr are obtained under the C1 condition respectively. 0.3%, 0.3% and 0.4% bitrate reduction for luma, chroma Cb and Cr are obtained under the C2 condition respectively. In terms of computational complexity, the encoding time increases by 6% while the decoding time increases by 10%.

To further evaluate the prediction effect of the proposed optimization scheme, we also count the errors during the transform domain prediction stage. Specifically, for each sequence in Cat1, prediction errors of all slices are accumulated if the upsampled prediction is enabled. As illustrated in Fig. 6, the average prediction errors of each type of point cloud are all smaller than that of the original prediction scheme in TMC13-v22.0. Therefore, our proposed method can effectively improve compression efficiency by reducing prediction errors.

5 Conclusions

In this paper, a subnode-based prediction is proposed to improve the lossy point cloud attribute compression for the MPEG G-PCC platform. Based on the original upsampled transform domain prediction scheme, we leverage some already-encoded neighbor nodes at the same level as the current node to be encoded to optimize the original prediction

▼ **Table 3. Performance of the proposed method against GeSTM-v2.0 under C1 and C2 configurations**

Dataset Category	C1 BD-Rate/%			C2 BD-Rate/%		
	L	Cb	Cr	L	Cb	Cr
Cat2-A average	−0.4	−0.5	−0.5	−0.3	−0.3	−0.4
Cat2-B average	−0.3	−0.3	−0.3	−0.2	−0.2	−0.2
Cat2-C average	−0.5	−0.4	−0.5	−0.4	−0.4	−0.3
Overall average	**−0.4**	**−0.4**	**−0.5**	**−0.3**	**−0.3**	**−0.4**
Avgerage encoding/ decoding time (%)	106/109			101/110		

BD: Bjontegaard delta

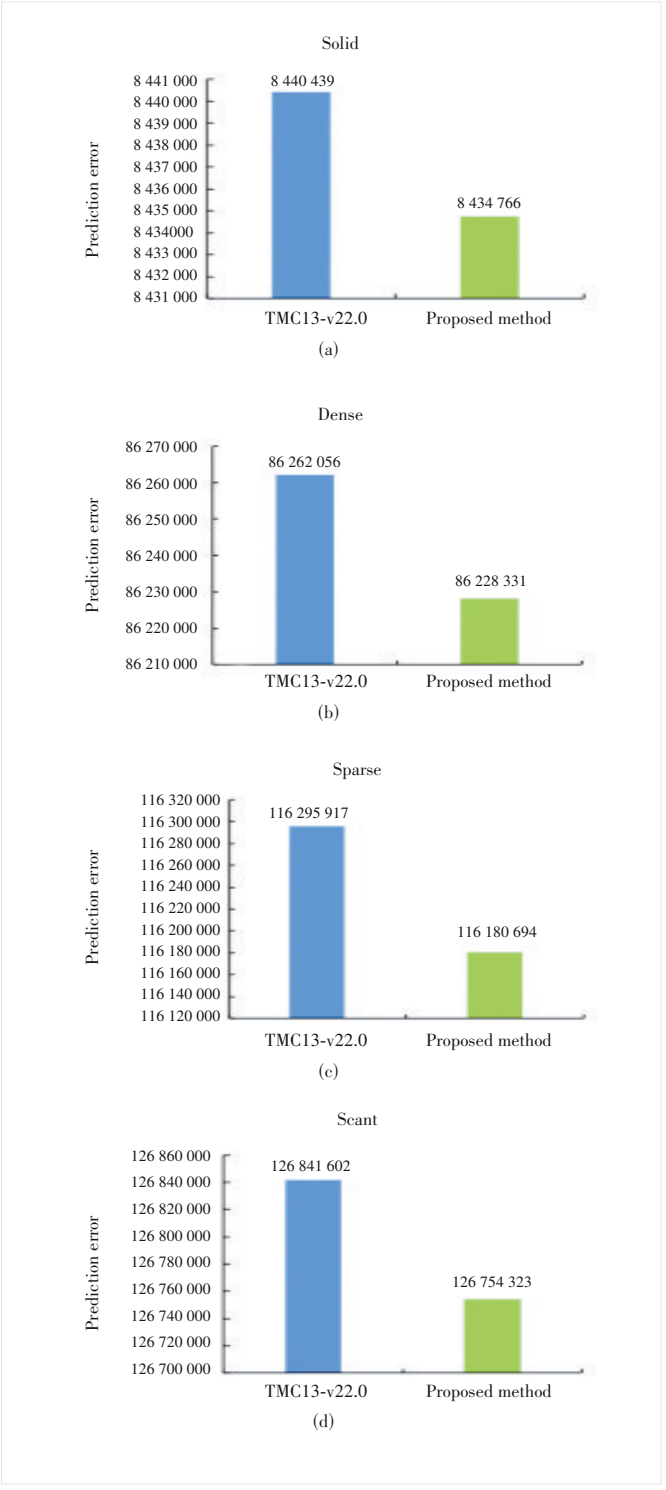

▲ **Figure 6. Prediction errors of the proposed method compared with the original prediction scheme in geometry-based point cloud compression (G-PCC) (i.e., reference software TMC13-v22.0)**

process. Additionally, a more refined prediction reference relationship is introduced based on the geometric distribution among neighbor nodes. Extensive simulation results demonstrate that our proposed method can achieve consistent coding gains on all types of point clouds, whether sparse LiDAR point clouds, dense colored point clouds, or multi-attribute point clouds, compared to the latest G-PCC test models.

References

[1] TULVAN C, MEKURIA R, LI Z. Use cases for point cloud compression (PCC), output document N16331 [R]. Geneva, Switzerland: ISO/IEC JTC 1/SC29/WG 11 MPEG, 2016
[2] MEKURIA R, BLOM K, CESAR P. Design, implementation, and evaluation of a point cloud codec for tele-immersive video [J]. IEEE transactions on circuits and systems for video technology, 2017, 27(4): 828 – 842. DOI: 10.1109/TCSVT.2016.2543039
[3] MPEG 3D Graphics Coding Group. Call for proposals for point cloud coding v2, output document N16763 [R]. 2017
[4] MPEG 3D Graphics and Haptics Coding Group. V-PCC test model v22, output document N00572 [R]. Antalya, Turkish: ISO/IEC JTC 1/SC 29/WG 11 MPEG, 2023
[5] MPEG 3D Graphics and Haptics Coding Group. G-PCC test model v22, output document N00571 [R]. Antalya, Turkish: ISO/IEC JTC 1/SC 29/WG 11 MPEG, 2023
[6] SCHNABEL R, KLEIN R. Octree-based point-cloud compression [C]//Symposium on Point-Based Graphics. Eurographics Association, 2006: 111 – 120. DOI: 10.2312/SPBG/SPBG06/111-120
[7] PENG J L, KUO C C J. Progressive geometry encoder using octree-based space partitioning [C]//2004 IEEE International Conference on Multimedia and Expo (ICME). IEEE, 2004: 1 – 4. DOI: 10.1109/ICME.2004.1394110
[8] NAKAGAMI O. Report on triangle soup decoding, input document m52279 [R]. Brussels, Belgium: ISO/IEC JTC 1/SC 29/WG 11 MPEG, 2020
[9] FLYNN D, TOURAPIS A, MAMMOU K. Predictive geometry coding, input document m51012 [R]. Geneva, Switzerland: ISO/IEC JTC 1/SC 29/WG11 MPEG, 2019
[10] MAMMOU K. PCC test model category 3 v0, output document N17249 [R]. Macau, China: ISO/IEC JTC 1/SC 29/WG 11 MPEG, 2017
[11] CHOU P A, DE QUEIROZ R. L. Transform coder for point cloud attributes, input document m38674 [R]. Geneva, Switzerland: ISO/IEC JTC 1/SC29/WG 11 MPEG, 2016
[12] DE QUEIROZ R L, CHOU P A. Compression of 3D point clouds using a region-adaptive hierarchical transform [J]. IEEE transactions on image processing, 2016, 25(8): 3947 – 3956. DOI: 10.1109/TIP.2016.2575005
[13] FLYNN D, LASSERRE S. G-PCC CE13.18 report on upsampled transform domain prediction in RAHT, input document m49380 [R]. Gothenburg, Sweden: ISO/IEC JTC 1/SC 29/WG 11 MPEG, 2019
[14] WANG W, XU Y, ZHANG Ket al. Sub-node-based prediction in transform domain for RAHT, input document m60203 [R]. Online: ISO/IEC JTC 1/SC 29/WG 11 MPEG, 2022
[15] MAMMOU K. Point cloud compression core experiment 13.6 on attributes prediction strategies, output document N18007 [R]. Macau, China: ISO/IEC JTC 1/SC 29/WG 11 MPEG, 2018
[16] MAMMOU K, TOURAPIS A, KIM J, et al. Proposal for improved lossy compression in TMC1, input document m42640 [R]. San Diego, United states: ISO/IEC JTC 1/SC 29/WG 11 MPEG, 2018
[17] WEI H L, SHAO Y T, WANG J, et al. Enhanced intra prediction scheme in point cloud attribute compression [C]//2019 IEEE Visual Communications and Image Processing (VCIP). IEEE, 2019: 1 – 4. DOI: 10.1109/VCIP47243.2019.8966001
[18] YEA S. VOSOUGHI A, LIU S. Bilateral filtering for predictive transform in G-PCC, input document m46365 [R]. Marrakech, Morocco: ISO/IEC JTC1/SC 29/WG 11 MPEG, 2019
[19] YIN Q, REN Q S, ZHAO L L, et al. Lossless point cloud attribute compression with normal-based intra prediction [C]//2021 IEEE International Symposium on Broadband Multimedia Systems and Broadcasting (BMSB). IEEE, 2021: 1 – 5. DOI: 10.1109/BMSB53066.2021.9547021
[20] ZHANG X M, WAN W G, AN X D. Clustering and DCT based color point cloud compression [J]. Journal of signal processing systems, 2017, 86(1): 41 – 49. DOI: 10.1007/s11265-015-1095-0
[21] COHEN R A, TIAN D, VETRO A. Point cloud attribute compression using 3-D intra prediction and shape-adaptive transforms [C]//2016 Data Compression Conference (DCC). IEEE, 2016: 141 – 150. DOI: 10.1109/DCC.2016.67
[22] WANG L J, WANG L Y, LUO Y T, et al. Point-Cloud compression using data independent method—a 3D discrete cosine transform approach [C]//2017 IEEE International Conference on Information and Automation (ICIA). IEEE, 2017: 1 – 6. DOI: 10.1109/icinfa.2017.8078873
[23] ZHANG C, FLORÊNCIO D, LOOP C. Point cloud attribute compression with graph transform [C]//2014 IEEE International Conference on Image Processing (ICIP). IEEE, 2014: 2066 – 2070. DOI: 10.1109/ICIP.2014.7025414
[24] SHAO Y T, ZHANG Z B, LI Z, et al. Attribute compression of 3D point clouds using Laplacian sparsity optimized graph transform [C]//2017 IEEE Visual Communications and Image Processing (VCIP). IEEE, 2017: 1 – 4. DOI: 10.1109/VCIP.2017.8305131
[25] XU Y Q, HU W, WANG S S, et al. Cluster-based point cloud coding with normal weighted graph Fourier transform [C]//2018 IEEE International Conference on Acoustics, Speech and Signal Processing (ICASSP). IEEE, 2018: 1753 – 1757. DOI: 10.1109/ICASSP.2018.8462684
[26] XU Y Q, HU W, WANG S S, et al. Predictive generalized graph Fourier transform for attribute compression of dynamic point clouds [J]. IEEE transactions on circuits and systems for video technology, 2021, 31(5): 1968 – 1982. DOI: 10.1109/TCSVT.2020.3015901
[27] HOODA R, PAN W D. Early termination of dyadic region-adaptive hierarchical transform for efficient attribute compression of 3D point clouds [J]. IEEE signal processing letters, 2022, 29: 214 – 218. DOI: 10.1109/LSP.2021.3133204
[28] MPEG 3D Graphics and Haptics Coding Group. TMC13 software repository [EB/OL]. (2023-06-02)[2023-11-20]. http://mpegx.int-evry.fr/software/MPEG/PCC/TM/mpeg-pcc-tmc13/-/tags/release-v22.0-rc1
[29] MPEG 3D Graphics and Haptics Coding Group. GeS-TM software repository [EB/OL]. (2023-06-05)[2023-11-20]. http://mpegx.int-evry.fr/software/MPEG/PCC/TM/mpeg-pcc-ges-tm/-/tree/ges-tm-v2.0-rc2
[30] MPEG 3D Graphics and Haptics Coding Group. Common test conditions for G-PCC, output document N00578 [R]. Antalya, Turkish: ISO/IEC JTC 1/SC29/WG 11 MPEG, 2023
[31] MPEG 3D Graphics and Haptics Coding Group. MPEG content repository [EB/OL]. (2023-03-17)[2023-11-20]. http://mpegfs.int-evry.fr/mpegcontent

Biographies

YIN Qian received her MS degree in signal and information processing from University of Electronic Science and Technology of China in 2021. She is currently pursuing a PhD degree in computer science at Peking University, China. She is actively participating in the research work of the Audio Video Coding Standard (AVS) Workgroup of China and Moving Picture Experts Group (MPEG). Her research interests include video and point cloud compression.

ZHANG Xinfeng received his BS degree in computer science from Hebei University of Technology, China in 2007 and PhD degree in computer science from the Institute of Computing Technology, Chinese Academy of Sciences in 2014. From 2014 to 2017, he was a research fellow with the Rapid-Rich Object Search

Lab, Nanyang Technological University, Singapore. From October 2017 to October 2018, he was a postdoctoral fellow with the School of Electrical Engineering System, University of Southern California, Los Angeles, USA. From December 2018 to August 2019, he was a research fellow with the Department of Computer Science, City University of Hong Kong, China. He is currently an assistant professor with the School of Computer Science and Technology, University of Chinese Academy of Sciences. He has authored more than 150 refereed journal/conference papers. His research interests include video compression and processing, image/video quality assessment, and 3D point cloud processing.

HUANG Hongyue received his BE degree in communication engineering from Beijing University of Posts and Telecommunications, China in 2015, MS degree in computer science from the Technical University of Berlin (TUB), Germany in 2018, and PhD degree in computer science from the Free University of Brussels (VUB), Belgium in 2021. He is currently a postdoctoral researcher with the National Engineering Research Center of Visual Technology, Peking University, China. His research interests include inventing and optimizing deep-learning-based compression methods for 2D images/videos and 3D visual content such as immersive videos, point clouds, and light field images.

WANG Shanshe received his BS degree from the Department of Mathematics, Heilongjiang University, China in 2004, MS degree in computer software and theory from Northeast Petroleum University, China in 2010, and PhD degree in computer science from the Harbin Institute of Technology, China. He held a postdoctoral position with Peking University, China from 2016 to 2018. He is currently an associate researcher with the School of Electronics Engineering and Computer Science, Institute of Digital Media, Peking University. His current research interests include video compression and image and video quality assessment.

MA Siwei (swma@stu.pku.edu.cn) received his BS degree from Shandong Normal University, China in 1999, and PhD degree in computer science from the Institute of Computing Technology, Chinese Academy of Sciences in 2005. He held a postdoctoral position with the University of Southern California, Los Angeles, USA from 2005 to 2007. He is currently a professor with the School of Electronics Engineering and Computer Science, Institute of Digital Media, Peking University, China. He has authored over 300 technical articles in refereed journals and proceedings in image and video coding, video processing, video streaming, and transmission. He served/serves as an associate editor for the *IEEE Transactions on Circuits and Systems for Video Technology* and *Journal of Visual Communication and Image Representation*.